HHS Public Access

Author manuscript

J Neurosurg. Author manuscript; available in PMC 2019 June 01.

Published in final edited form as:

J Neurosurg. 2018 June ; 128(6): 1690–1697. doi:10.3171/2017.1.JNS162061.

Red-light excitation of protoporphyrin IX fluorescence for subsurface tumor detection

David W. Roberts, MD[1,2,3,4], **Jonathan D. Olson, BS**[4], **Linton T. Evans, MD**[1], **Kolbein K. Kolste, PhD**[4], **Stephen C. Kanick, PhD**[4], **Xiaoyao Fan, PhD**[1,4], **Jaime J. Bravo, BS**[4], **Brian C. Wilson, PhD**[5], **Frederic Leblond, PhD**[6,7], **Mikael Marois, BE**[4], and **Keith D. Paulsen, PhD**[1,3,4]

[1]Section of Neurosurgery, Dartmouth-Hitchcock Medical Center, Lebanon

[2]Geisel School of Medicine, Dartmouth College, Hanover, New Hampshire

[3]Norris Cotton Cancer Center, Dartmouth-Hitchcock Medical Center, Lebanon

[4]Thayer School of Engineering, Dartmouth College, Hanover, New Hampshire

[5]Princess Margaret Cancer Centre/University Health Network and Department of Medical Biophysics, University of Toronto, Ontario

[6]Department of Engineering Physics, Polytechnique Montreal, Quebec

[7]Centre de Recherche du Centre Hospitalier de l'Université de Montréal, Quebec, Canada

Abstract

OBJECTIVE—The objective of this study was to detect 5-aminolevulinic acid (ALA)-induced tumor fluorescence from glioma below the surface of the surgical field by using red-light illumination.

METHODS—To overcome the shallow tissue penetration of blue light, which maximally excites the ALA-induced fluorophore protoporphyrin IX (PpIX) but is also strongly absorbed by hemoglobin and oxyhemoglobin, a system was developed to illuminate the surgical field with red light (620–640 nm) matching a secondary, smaller absorption peak of PpIX and detecting the fluorescence emission through a 650-nm longpass filter. This wide-field spectroscopic imaging system was used in conjunction with conventional blue-light fluorescence for comparison in 29 patients undergoing craniotomy for resection of high-grade glioma, low-grade glioma, meningioma, or metastasis.

Correspondence: David W. Roberts, Section of Neurosurgery, One Medical Center, Dr., Dartmouth-Hitchcock Medical Center, Lebanon, NH 03756. david.w.roberts@dartmouth.edu.

Clinical trial registration no.: NCT02191488 (clinicaltrials.gov)

Disclosures

Drs. Leblond (with Dartmouth College and Polytechnique Montreal), Paulsen (with Dartmouth College), Roberts (with Dart-mouth College), and Wilson (with University Health Network, Toronto) are patent holders and have patent applications on several aspects of the fluorescence technologies discussed in this study.

Author Contributions

Conception and design: Roberts, Olson, Kolste, Wilson, Leblond, Paulsen. Acquisition of data: Roberts, Olson, Evans, Kolste, Fan, Bravo. Analysis and interpretation of data: all authors. Drafting the article: Roberts, Fan. Critically revising the article: Olson, Evans, Kanick, Fan, Bravo, Wilson, Leblond, Paulsen. Reviewed submitted version of manuscript: all authors. Approved the final version of the manuscript on behalf of all authors: Roberts. Statistical analysis: Olson. Administrative/technical/material support: Roberts, Olson, Kolste, Fan, Bravo. Study supervision: Roberts, Paulsen.

RESULTS—Although, as expected, red-light excitation is less sensitive to PpIX in exposed tumor, it did reveal tumor at a depth up to 5 mm below the resection bed in 22 of 24 patients who also exhibited PpIX fluorescence under blue-light excitation during the course of surgery.

CONCLUSIONS—Red-light excitation of tumor-associated PpIX fluorescence below the surface of the surgical field can be achieved intraoperatively and enables detection of subsurface tumor that is not visualized under conventional blue-light excitation.

Keywords

5-aminolevulinic acid; fluorescence-guided surgery; protoporphyrin IX; brain tumor; glioma; meningioma; metastasis; optical spectroscopy; oncology

5–Aminolevulinic Acid (ALA)–induced protoporphyrin IX (PpIX) fluorescence for guidance in the resection of intracranial tumor has generated considerable interest over the past decade, and Class I evidence supports its ability to facilitate more complete tumor resection and improve 6-month progression-free survival.[16] Since the publication of a multiinstitutional trial in 2006,[16] a growing number of clinical studies have confirmed the technology's utility and potential for wider applicability.[12–15,17,21,22,25]

Currently, ALA-induced fluorescence imaging utilizes blue-violet light (405 nm) excitation of PpIX, corresponding to the largest absorption peak of the fluorophore. The resulting fluorescence is most intense in the red portion of the light spectrum, with a peak at around 635 nm and extending to about 720 nm. These excitation and detection wavelengths have been incorporated into operating microscopes through add-on modules that have made the acquisition and interpretation of fluorescence intuitive and minimally disruptive to the surgical workflow.

A limitation of the current clinical application, however, is the inability of this blue excitation light to appreciably penetrate tissue beyond the exposed tissue surface of the surgical field (submillimeters), primarily because of very strong attenuation by hemoglobin (Fig. 1). Thus, tumor tissue that would otherwise fluoresce is not detectable if it is overlaid by nonfluorescent tissue or blood. Hemoglobin absorption is markedly reduced at longer (red) wavelengths, and red excitation should improve the detection of tumor-associated fluorophores to greater depths below the accessible tissue surface. In this paper, we report our experience in 29 patients of using red-light excitation at 630 nm and detection in the range of 650–720 nm and making intraoperative comparisons with blue-light excitation at approximately 405 nm and detection in the range of 600–720 nm.

Methods

Patient Selection

This study adhered to the principles set forth in the US Code of Federal Regulations, Title 45, Part 46, Protection of Human Subjects, revised January 15, 2009 (http://www.hhs.gov/ohrp/humansubjects/guidance/45cfr46.html), and the World Medical Association Declaration of Helsinki (http://jamanetwork.com/journals/jama/fullarticle/1760318). It was registered with the ClinicalTrials.gov database (http://clinicaltrials.gov), and its registration

no. is NCT02191488. Patients were enrolled under an institutional review board–approved FDA Investigational New Drug protocol for ALA-induced fluorescence in intracranial tumor between April 2015 and February 2016. Subjects were 21 years or older, were preoperatively diagnosed with low- or high-grade glioma, meningioma, or intracranial metastatic tumor, and satisfied standard inclusion and exclusion criteria for ALA studies.[13] Maximum safe resection of tumor defined by T1-weighted MRI with gadolinium enhancement or of nonenhancing tumor demonstrated on T2-weighted imaging was the goal in all surgeries. Signed informed consent was obtained for all patients.

Microscope Adaptation

Implementation of red-light fluorescence imaging required adaptation of an OPMI Pentero operating microscope (Carl Zeiss Surgical GmbH) that was already equipped with a Blue 400 module (Carl Zeiss AG) for fluorescence imaging.[23] To provide red-light excitation of the surgical field, a customized filter platform was attached at the objective lens of the microscope. This customization did not interfere with conventional draping or functions of the operating microscope. The attachment enabled a 630 ± 10–nm bandpass filter (ET630/20×, Chroma Technology Corp.) to be manually slid into and out of the xenon arc lamplight path of the microscope (Fig. 2). The light source remained the regular white light xenon arc lamp of the microscope but in the manner described was filtered to allow only a subset of wavelengths to illuminate the surgical field. An imaging spectrometer, or a spectrally resolved camera, was connected to an existing optical side port on the microscope, as previously described.[23] Light was collected from the surgical field over an approximately 7-nm-wide spectral window via a liquid crystal tunable filter in the optical path of the adaptor tube holding the detection camera. An additional 650-nm longpass filter eliminated remaining excitation light passing through the tunable filter. The longpass filter was placed between the adaptor port and the tunable filter and manually rotated in and out of the optical path during red- and white- and/or blue-light imaging.

Fluorescence Overlay

To eliminate the display of PpIX below the detection limits, images acquired with the internal camera of the microscope were overlaid with the lower bound of the 95% confidence interval of PpIX concentration determined by the imaging system. This lower bound was calculated from the estimate of PpIX concentration and the noise present in the signal. For high signal-to-noise ratios, this lower bound was negligibly different from the actual PpIX estimate. For the overlay images under blue-light excitation, this lower bound was presented on a logarithmic false-color scale ranging from 0.05 μg/ml (blue) to 1 μg/ml (green) to 20 μg/ml (bright yellow). A quantitative estimate of the PpIX concentration is not yet available for red-light excitation, so we are reporting the intensity of the spectrally fit PpIX component present in the measured spectrum, and the color bar was based on the limit of detection and the saturation value of the camera. The same color scale was used for all patients. In this study, processing and filtering the optical data took less than 1 second, and image registration took almost 1 minute.

Study Protocol

Approximately 3 hours prior to surgery, patients took an oral dose of ALA (20 mg/kg, DUSA Pharmaceuticals Inc.). All surgeries were performed in an otherwise conventional manner using image guidance (StealthStation, Medtronic Navigation) coregistered to preoperative MRI. Craniotomies were placed directly over tumors unless the approach to that portion of the cranium required the opening to be off-center. Fluorescence imaging was performed before and after dural opening, upon tumor exposure, during resection, and at the completion of resection. White light as well as blue- and red-excitation fluorescence light images were obtained using the hyperspectral camera.[23] Additional measurements were made with a previously described handheld fiber optic probe for quantitative fluorophore detection.[24] Visual and red-light fluorescence determinations, MRI location, and histology were collected under coregistered conditions. The primary data analysis was a comparison of tissue fluorescence under blue-light and red-light conditions. Spectral fitting was used to separate the PpIX fluorescence from that of photoproducts and from background tissue autofluorescence, for both blue and red excitation. Confidence intervals[1] on parameter estimates were used to determine the quantifiable presence of fluorescence within the exposed surgical field.

Visual (subjective) fluorescence was graded by the surgeon as none (0), low (1), moderate (2), and high (3). For ease of comparison with the surgeon's fluorescence rating, measurements taken by the fluorescence imaging spectrometer were grouped into 4 rankings (0–3). These rankings were determined by comparing the maximum concentration or intensity observed during the case to fixed thresholds. For this study, the maximum was defined as the average signal over a square region 11 pixels wide and centered on the maximum signal observed during the case. For PpIX excited by blue light (approximately 405 nm), the signal was defined as the quantitative estimate of PpIX in μg/ml with thresholds of 0.03, 0.15, and 0.60 μg/ml for rankings 1, 2, and 3, respectively. For PpIX excited by red light (approximately 635 nm), the signal was defined as the intensity of the spectrally fit PpIX component present in the measured spectrum. The thresholds for red-light–excited PpIX were 0.5, 2, and 4 AUs for rankings 1, 2, and 3, respectively. This system was used in place of a quantitative estimate because a method to remove the confounding effects of optical properties and detection at depth has not yet been developed and validated for red light.

MRI Data Reconstruction

An intraoperative stereovision (iSV) system that consisted of 2 charge-coupled device (CCD) cameras (Flea2, Point Grey Research Inc.) was attached to the operating microscope (OPMI Pentero, Carl Zeiss Surgical GmbH). The operating microscope was connected to a commercial navigation system (StealthStation S7, Medtronic) for optical tracking, and fiducial-based registration was performed on the navigation system at the beginning of surgery to provide intraoperative navigation. The camera parameters of the iSV system were precalibrated for 3D surgical surface reconstruction. The technical details have been reported elsewhere.[5,6,18,20]

Before and after dural opening, a pair of iSV images of the surgical field was acquired and a 3D surface was reconstructed and coregistered with MRI using methods described previously[2] and briefly summarized here. Specifically, the brain was segmented on the MR images using a level-set algorithm,[26] with manual refinement in the craniotomy region to include features on the brain surface. The iSV surface was projected along the average surface normal (the line perpendicular to the plane tangential to the surface) onto the segmented brain surface, and a point cloud that geometrically matched the brain surface was produced to compensate for brain deformation. An MRI-encoded texture map was generated by replacing iSV pixel values with MRI intensities at the projected locations. The texture map was created by translating successively along the surface normal from 0 to 5 mm below the surgical surface. The pixel intensities in the generated MR images were a weighted average over a depth representative of the penetration of the excitation light wavelengths.

Results

Twenty-nine patients undergoing craniotomy for resection of tumor were included in this study. Tumor pathologies included glioblastoma (GBM; 10 patients), anaplastic astrocytoma (1), anaplastic oligoastrocytoma (1), diffuse astrocytoma (3), ganglioglioma (2), metastatic tumor (4), meningioma WHO Grade I (4), atypical meningioma WHO Grade II (1), anaplastic meningioma WHO Grade III (1), and preoperatively presumed tumors (2) that on final pathology were nonneoplastic (an ectopic bone formation and a meningioangiomatosis).

Tables 1–4 summarize the fluorescence characteristics observed during surgery, grouped by high-grade gliomas, low-grade gliomas, meningiomas, and metastases. All GBMs demonstrated fluorescence under both blue- and red-light illumination. Low levels of fluorescence were detected quantitatively with blue-light illumination but not under red-light illumination in the anaplastic astrocytoma, the anaplastic oligoastrocytoma, and 1 of 3 low-grade astrocytomas. One fibrous meningioma (WHO Grade I) showed high fluorescence with blue- but not red-light excitation; the other 4 meningiomas as well as all 4 metastatic tumors exhibited fluorescence under both blue- and red-light illumination. In the 24 tumors in which fluorescence was visualized under blue-light illumination, fluorescence under red-light illumination was seen in 22, corresponding to tumor at depths up to 5 mm.

Most noteworthy are the findings that there was no evidence of fluorescence detection from tumor deeper than 1 mm under blue-light illumination and that fluorescence elicited by red-light illumination was weaker but consistent with contribution from PpIX up to 5 mm below the exposed tissue surface.

Illustrative Cases

Case 3

Following a generalized tonic-clonic seizure, a 68-year-old man presented with postictal left-sided weakness. Computed tomography and MRI demonstrated a 4-cm, ring-enhancing, right parietal intrinsic tumor most consistent with high-grade glioma (Fig. 3A), and the patient was brought to the operating room for resection. On elevation of the bone flap and

exposure of normal-appearing dura mater, visualization under blue light showed no fluorescence, and this was confirmed using the handheld fiber optic probe that has significantly higher sensitivity. Under red-light illumination, strong fluorescence was detected in the inferior aspect of the dural exposure (Fig. 3D). Upon opening of the dura, tumor extending to the cortex in the area underlying the region positive for red-excitation fluorescence was observed under white-light illumination, and this tissue then fluoresced under both blue- and red-light excitation (Fig. 4). Of note, the location and distribution of the red-light fluorescence detected prior to dural opening corresponded to those on both the blue- and red-excitation fluorescence observed after the dura was open. Moreover, the red-excitation fluorescence maps closely matched the shape of enhancement on MRI over a 5-mm-deep section, while the blue-light map matched the MRI over a 1-mm-deep section only after the dura was removed. Postoperative MRI showed complete resection of contrast-enhancing tumor. Pathology confirmed the diagnosis of GBM.

Case 11

A 54-year-old right-handed woman presented with a history of headaches over the prior 2 weeks. Her neurological examination was normal. Magnetic resonance imaging demonstrated a 4.5-cm, contrast-enhancing, right middle fossa extraaxial mass consistent with meningioma (Fig. 5A). At surgery, no fluorescence under blue or red illumination was demonstrated on exposure of the dura (the tumor and involved dura lying more than 5 mm inferomedially). Upon opening of the dura, an extraaxial mass was visible under white light and showed positive fluorescence under both blue- and red-light excitation. The lateral aspect of the tumor was covered by a small amount of thickened arachnoid and blood, and this area did not fluoresce under blue light; under red light, a broader area of tumor fluorescence was documented (Fig. 5B–D). The PpIX fluorescence maps from red- and blue-light excitation corresponded to the map of MRI enhancement over the 5- and 1-mm depths, respectively (Fig. 5E and F). Complete resection of contrast-enhancing tumor was demonstrated on postoperative MRI. The final pathological diagnosis was atypical meningioma (WHO Grade II).

Case 24

A 57-year-old woman developed headache and speech difficulty over the preceding 2 weeks and on neurological examination was without focal or lateralized findings apart from slowed speech. Magnetic resonance imaging showed a 5.5-cm, rim-enhancing, left frontal mass lesion (Fig. 6A). An awake craniotomy for tumor resection was performed without complication. During surgery, blue-light illumination of the exposed cortical surface produced visible fluorescence; red illumination also produced detectable fluorescence, including areas of tumor involvement beneath a thin layer of nonfluorescent cortex and not revealed under blue light (Fig. 6B–D). Spectral data acquired using the handheld fiber optic probe from these areas demonstrated no PpIX signal under blue-light excitation but a robust PpIX signal under red-light exposure (Fig. 6E). The necrotic central portion of the tumor did not show fluorescence under either blue- or red-light illumination. Postoperative MRI confirmed complete resection and no residual contrast enhancement. Pathology confirmed the preoperative diagnosis of GBM.

Discussion

Fluorescence guidance using ALA has demonstrated substantial utility in the resection of intracranial malignant glioma, as well as potential applicability in other pathologies such as meningioma and metastatic tumor.[7,21,24] Standard clinical practice involves the use of an adapted operating microscope capable of illuminating the surgical field with blue light and equipped with appropriate filters for optimal visualization of the fluorescence emitted by PpIX. One limitation of this technique, however, is that the blue-excited PpIX fluorescence returns a signal that detects fluorophore only within the most superficial 1 mm or less of tissue. This limitation is an important consideration for surgical guidance since tumor that is covered by nonfluorescent tissue or by a thin layer of blood—conditions common in a surgery for intracranial tumor resection—is not likely to be detected. Blue-light excitation illuminates PpIX at its wavelength of maximum absorption, although this portion of the spectrum also overlaps with strong absorption from hemoglobin (Fig. 1). Deeper sampling of PpIX can be achieved through the use of deeper-penetrating red light, where attenuation from absorption by blood is reduced, although PpIX is a less efficient absorber at red wavelengths. These properties underpin the approach used in the present study, and the results highlight this trade-off in depth versus efficiency.

Previous studies exploring the ability of red-light–excited fluorescence to detect subsurface PpIX in tissue-simulation phantoms have demonstrated PpIX detection at depths of up to 5 mm, with either a fiber optic point-spectroscopy probe or a wide-field imaging system.[4,10] Fluorophore visualization at such a depth may well have practical benefit, countering the common obscuration of parts of the resection surface by blood or necrotic tissue. Strategies, instrumentation, and algorithms capable of assessing the depth and quantity of subsurface fluorophore are under development.[10,11,19] Studies in rodent tumor models have confirmed the feasibility of the approach, with both fiber-optic probes and wide-field imaging. In a CNS-1 rodent tumor model, PpIX fluorescence from depths of 3 mm was detectable using the same operating microscope adaptation used in the present study (Kolste et al., unpublished data, 2015). Wide-field interrogation of the surgical field is essential for workflow efficiency during surgery. The concept of tuning the excitation source to provide a description of the topographic distribution of fluorophores has been tested preclinically but has yet to be evaluated clinically.[8,9]

Disadvantages of red-light fluorescence imaging include the following. First, additional modifications to the operating microscope are required to provide red-light illumination and incorporate the appropriate detection filters. The emission wavelengths detected with this method occur at the limits of human visual perception where the sensitivity is minimal, so that the approach is unlikely to provide fluorescence that is visible to the human eye without specialized equipment for detection and display. In this study, image processing and display were accomplished in approximately 1 minute but not in real time. The total time has now been reduced to approximately 10 seconds, and it is anticipated that this time delay will be substantially reduced in the near future. Second, quantitative interpretation of red-excited PpIX fluorescence is more complicated than that of blue-excited fluorescence since the images are influenced by both the concentration and the depth distribution of the PpIX, as well as by attenuation from absorption and scattering within the tissue. Modeling and

experimental studies of these issues are in progress. Third, imaging with red-light excitation is intrinsically less sensitive since the PpIX absorption is much reduced; thus, the threshold PpIX concentration for detection is higher. In part, this reduced sensitivity can be offset by increasing the excitation light intensity (the maximum intensity of which the system used in this study is capable, measured in mW/cm^2, is only 6.25% of that of the microscope's standard white-light source because of the interposed filter) and/or by using more sensitive (but more expensive) imaging detectors. For this investigation, the excitation light was obtained by filtering the existing white-light source. One beneficial consequence of exciting PpIX where its absorption is approximately 5% of that at 405 nm is the proportionate decrease in undesirable quenching of the fluorophore. Last, the fluorescence quantum yield of PpIX is low (approximately 0.06).[3] Fluorophores with considerably higher quantum yields (for example, Alexa Fluor, with a quantum yield of 0.3) are under investigation and will potentially yield brighter images, have a lower concentration threshold for detection, and likely prove useful in future applications.

Conclusions

A strategy for ALA-induced fluorescence guidance using red-light illumination of the surgical field and detection of fluorophore emission has been implemented and investigated during surgery for intracranial tumor resection in 29 patients. The technique enables subsurface detection of PpIX in tumor tissue not visualized under conventional blue-light excitation. The clinical utility of such a strategy and whether the required equipment modifications and the consequent indirect visualization are supported by such utility warrant further investigation.

Acknowledgments

This work was supported in part by NIH Grant No. R01NS052274 (D.W.R.) awarded by the National Institute of Neurological Disorders and Stroke and Grant No. K25CA138578 (F.L.) awarded by the National Cancer Institute. Carl Zeiss Surgical GmbH and Medtronic Navigation provided the fluorescence-enabled OPMI Pentero operating microscope and StealthStation navigation system, respectively. DUSA Pharmaceuticals supplied the ALA.

ABBREVIATIONS

ALA	5-aminolevulinic acid
GBM	glioblastoma
iSV	intraoperative stereovision
PpIX	protoporphyrin IX

References

1. Amelink A, Robinson DJ, Sterenborg HJ. Confidence intervals on fit parameters derived from optical reflectance spectroscopy measurements. J Biomed Opt. 2008; 13:054044. [PubMed: 19021424]
2. Fan X, Ji S, Hartov A, Roberts DW, Paulsen KD. Stereovision to MR image registration for cortical surface displacement mapping to enhance image-guided neurosurgery. Med Phys. 2014; 41:102302. [PubMed: 25281972]

3. Gouterman M, Khalil GE. Porphyrin free base phosphorescence. J Mol Spectrosc. 1974; 53:88–100.
4. Jermyn M, Kolste K, Pichette J, Sheehy G, Angulo-Rodríguez L, Paulsen KD, et al. Macroscopic-imaging technique for subsurface quantification of near-infrared markers during surgery. J Biomed Opt. 2015; 20:036014. [PubMed: 25793562]
5. Ji S, Fan X, Roberts DW, Paulsen KD. Efficient stereo image geometrical reconstruction at arbitrary camera settings from a single calibration. Med Image Comput Comput Assist Interv. 2014; 17:440–447. [PubMed: 25333148]
6. Ji SB, Fan XY, Roberts DW, Hartov A, Paulsen KD. Flow-based correspondence matching in stereovision. Lect Notes Comput Sci. 2013; 8184:106–113.
7. Kamp MA, Grosser P, Felsberg J, Slotty PJ, Steiger HJ, Reifenberger G, et al. 5-aminolevulinic acid (5-ALA)-induced fluorescence in intracerebral metastases: a retrospective study. Acta Neurochir (Wien). 2012; 154:223–228. [PubMed: 22080159]
8. Kanick SC, Davis SC, Zhao Y, Hasan T, Maytin EV, Pogue BW, et al. Dual-channel red/blue fluorescence dosimetry with broadband reflectance spectroscopic correction measures protoporphyrin IX production during photodynamic therapy of actinic keratosis. J Biomed Opt. 2014; 19:75002. [PubMed: 24996661]
9. Kim A, Roy M, Dadani FN, Wilson BC. Topographic mapping of subsurface fluorescent structures in tissue using multiwavelength excitation. J Biomed Opt. 2010; 15:066026. [PubMed: 21198200]
10. Kolste KK, Kanick SC, Valdés PA, Jermyn M, Wilson BC, Roberts DW, et al. Macroscopic optical imaging technique for wide-field estimation of fluorescence depth in optically turbid media for application in brain tumor surgical guidance. J Biomed Opt. 2015; 20:26002. [PubMed: 25652704]
11. Leblond F, Ovanesyan Z, Davis SC, Valdés PA, Kim A, Hartov A, et al. Analytic expression of fluorescence ratio detection correlates with depth in multi-spectral sub-surface imaging. Phys Med Biol. 2011; 56:6823–6837. [PubMed: 21971201]
12. Quick-Weller J, Lescher S, Forster MT, Konczalla J, Seifert V, Senft C. Combination of 5-ALA and iMRI in re-resection of recurrent glioblastoma. Br J Neurosurg. 2016; 30:313–317. [PubMed: 26743016]
13. Roberts DW, Valdés PA, Harris BT, Fontaine KM, Hartov A, Fan X, et al. Coregistered fluorescence-enhanced tumor resection of malignant glioma: relationships between δ-aminolevulinic acid-induced protoporphyrin IX fluorescence, magnetic resonance imaging enhancement, and neuropathological parameters. Clinical article. J Neurosurg. 2011; 114:595–603. [PubMed: 20380535]
14. Roessler K, Becherer A, Donat M, Cejna M, Zachenhofer I. Intraoperative tissue fluorescence using 5-aminolevolinic acid (5-ALA) is more sensitive than contrast MRI or amino acid positron emission tomography (^{18}F-FET PET) in glioblastoma surgery. Neurol Res. 2012; 34:314–317. [PubMed: 22449387]
15. Sanai N, Snyder LA, Honea NJ, Coons SW, Eschbacher JM, Smith KA, et al. Intraoperative confocal microscopy in the visualization of 5-aminolevulinic acid fluorescence in low-grade gliomas. J Neurosurg. 2011; 115:740–748. [PubMed: 21761971]
16. Stummer W, Pichlmeier U, Meinel T, Wiestler OD, Zanella F, Reulen HJ. Fluorescence-guided surgery with 5-aminolevulinic acid for resection of malignant glioma: a randomised controlled multicentre phase III trial. Lancet Oncol. 2006; 7:392–401. [PubMed: 16648043]
17. Stummer W, Rodrigues F, Schucht P, Preuss M, Wiewrodt D, Nestler U, et al. Predicting the “usefulness” of 5-ALA-derived tumor fluorescence for fluorescence-guided resections in pediatric brain tumors: a European survey. Acta Neurochir (Wien). 2014; 156:2315–2324. [PubMed: 25248327]
18. Sun H, Lunn KE, Farid H, Wu Z, Roberts DW, Hartov A, et al. Stereopsis-guided brain shift compensation. IEEE Trans Med Imaging. 2005; 24:1039–1052. [PubMed: 16092335]
19. Swartling J, Svensson J, Bengtsson D, Terike K, Andersson-Engels S. Fluorescence spectra provide information on the depth of fluorescent lesions in tissue. Appl Opt. 2005; 44:1934–1941. [PubMed: 15813529]
20. Tsai RY. A versatile camera calibration technique for high-accuracy 3D machine vision metrology using off-the-shelf TV cameras and lens. IEEE J Robot Autom. 1987; 3:323–344.

21. Valdes PA, Bekelis K, Harris BT, Wilson BC, Leblond F, Kim A, et al. 5-Aminolevulinic acid-induced protoporphyrin IX fluorescence in meningioma: qualitative and quantitative measurements in vivo. Neurosurgery. 2014; 10(Suppl 1):74–83. [PubMed: 23887194]
22. Valdés PA, Jacobs V, Harris BT, Wilson BC, Leblond F, Paulsen KD, et al. Quantitative fluorescence using 5-aminolevulinic acid-induced protoporphyrin IX biomarker as a surgical adjunct in low-grade glioma surgery. J Neurosurg. 2015; 123:771–780. [PubMed: 26140489]
23. Valdés PA, Leblond F, Jacobs VL, Wilson BC, Paulsen KD, Roberts DW. Quantitative, spectrally-resolved intraoperative fluorescence imaging. Sci Rep. 2012; 2:798. [PubMed: 23152935]
24. Valdés PA, Leblond F, Kim A, Harris BT, Wilson BC, Fan X, et al. Quantitative fluorescence in intracranial tumor: implications for ALA-induced PpIX as an intraoperative biomarker. J Neurosurg. 2011; 115:11–17. [PubMed: 21438658]
25. Widhalm G, Kiesel B, Woehrer A, Traub-Weidinger T, Preusser M, Marosi C, et al. 5-Aminolevulinic acid induced fluorescence is a powerful intraoperative marker for precise histopathological grading of gliomas with non-significant contrast-enhancement. PLoS One. 2013; 8:e76988. [PubMed: 24204718]
26. Wu Z, Paulsen KD, Sullivan JM Jr. Adaptive model initialization and deformation for automatic segmentation of T1-weighted brain MRI data. IEEE Trans Biomed Eng. 2005; 52:1128–1131. [PubMed: 15977742]

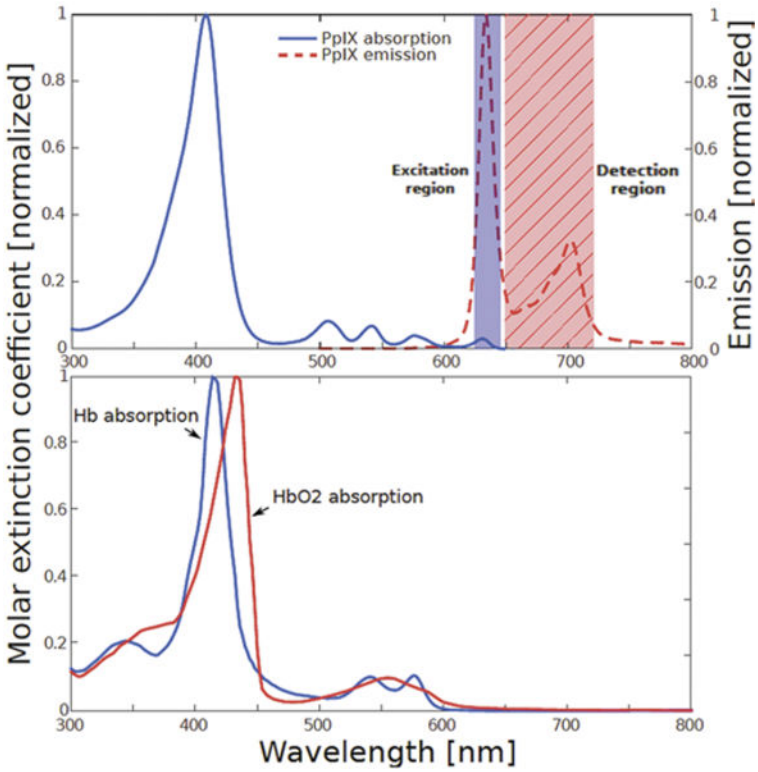

FIG. 1.

Upper: The portion of the PpIX absorption (excitation) spectrum corresponding to red illumination is indicated by the *shaded rectangle* labeled “Excitation region.” The portion of the PpIX emission spectrum detected during red-light illumination (the longer wavelength region of 650–720 nm) is indicated by the *hatched rectangle* labeled “Detection region.” **Lower:** The absorption spectra of deoxyhemoglobin (Hb) and oxyhemoglobin (HbO_2) showing the strong absorption in the blue wavelength region that limits tissue penetration. Figure is available in color online only.

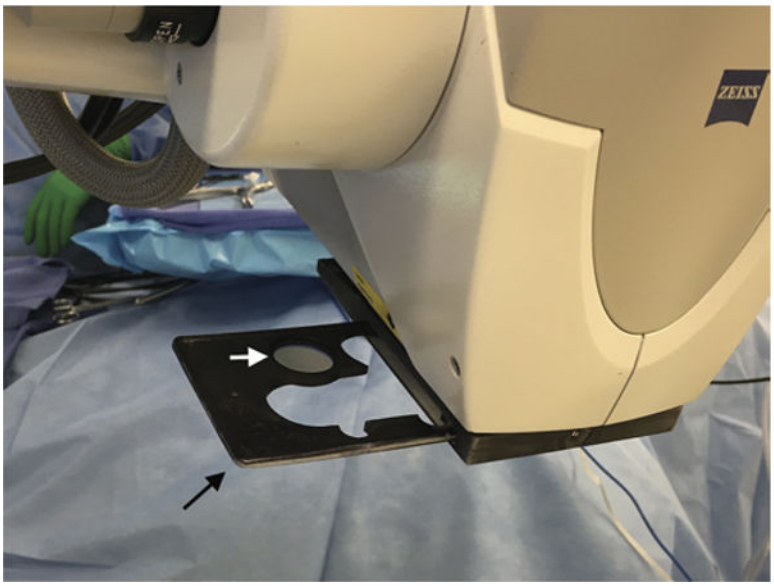

FIG. 2.

An adaptor (*black arrow*) attached at the objective lens of the operating microscope contains a 630 ± 10–nm bandpass filter (*white arrow*) that can be manually slid into and out of the xenon arc lamplight path of the microscope. Figure is available in color online only.

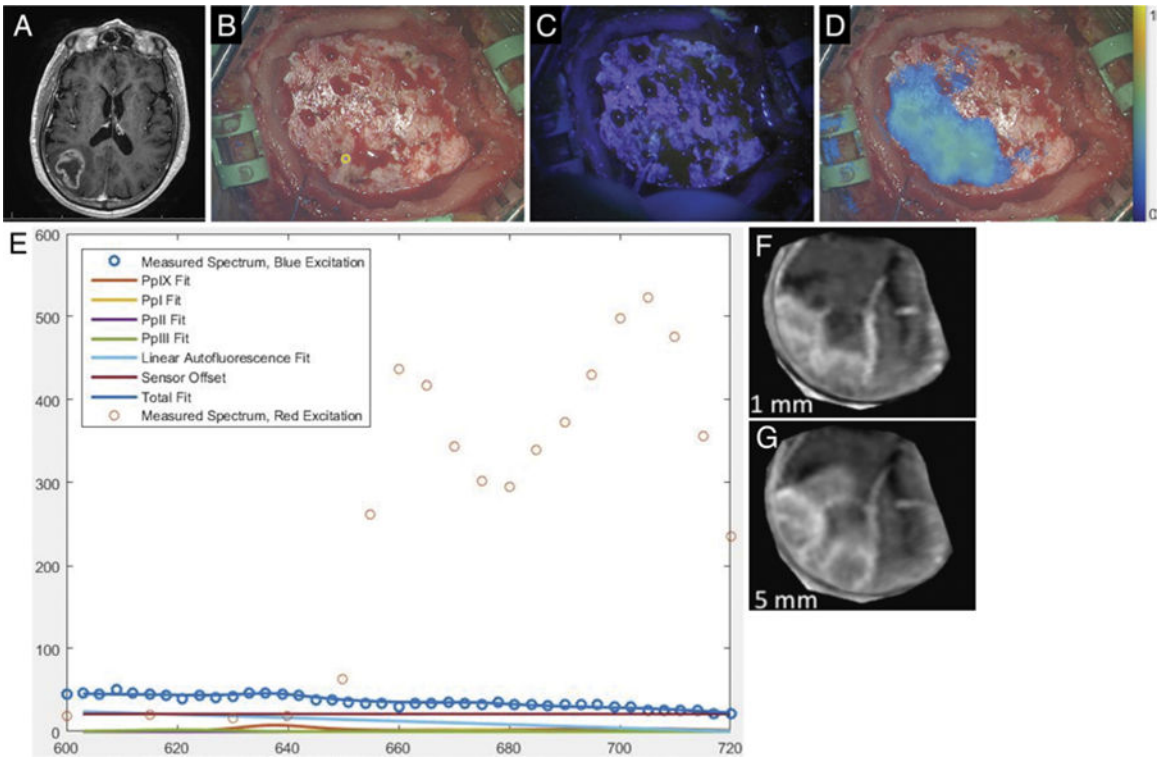

FIG. 3.

Case 3. **A:** Axial T1-weighted MR image showing a right parietal tumor. **B:** Under white-light visualization, the intact and normal-appearing dura has been exposed upon elevation of the free bone flap. (The *small yellow circle* in the lower middle portion of the figure corresponds to the site of handheld optical probe measurements, whose spectra are shown in panel E.) **C:** Under blue-light excitation, no red fluorescence is visible. **D:** Under red-light excitation, fluorescence (650–720 nm) corresponding to underlying tumor was detected and is displayed in a false color overlaid on the white-light image. **E:** The optical spectra acquired with the handheld optical probe and corresponding model fits for PpIX, photoproducts, and autofluorescence at the site indicated by the *small yellow circle* in panel B. The typical red emission peak of PpIX at 635 nm under blue-light excitation is absent, while emission at longer wavelengths is detected under red-light excitation, confirming the presence of PpIX. **F:** Reconstruction of weighted MRI data corresponding to a plane 0–1 mm below the dural surface in the operative field. **G:** Reconstruction of weighted MRI data corresponding to a plane 0–5 mm below the dural surface in the operative field.

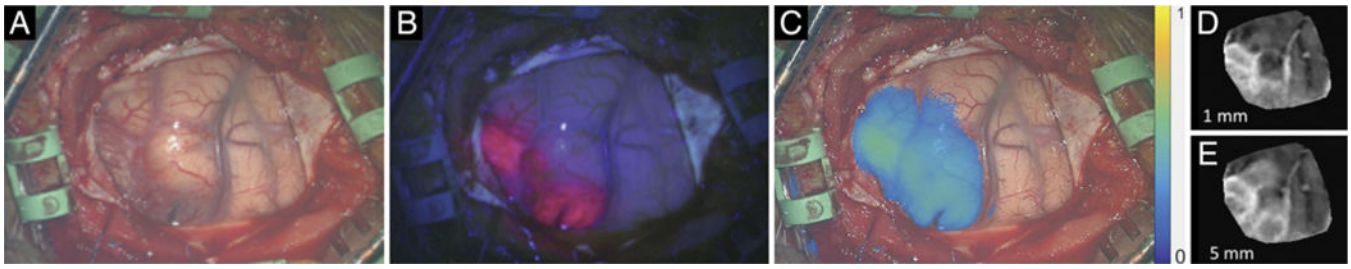

FIG. 4.

Case 3. **A:** The cortical surface under white-light illumination. **B:** Under blue light, red fluorescence is evident in tumor-involved cortex. **C:** Under red light, longer-wavelength fluorescence represented in a false color is more extensive, corresponding to the contribution from subsurface PpIX. The location and distribution of fluorescence detected before dural opening (in Fig. 3) are consistent with those demonstrated with the dura open. **D:** Reconstruction of MRI data corresponding to a weighted average of the first 1 mm below the cortical surface. **E:** Reconstruction of weighted MRI data corresponding to the first 5 mm below the cortical surface.

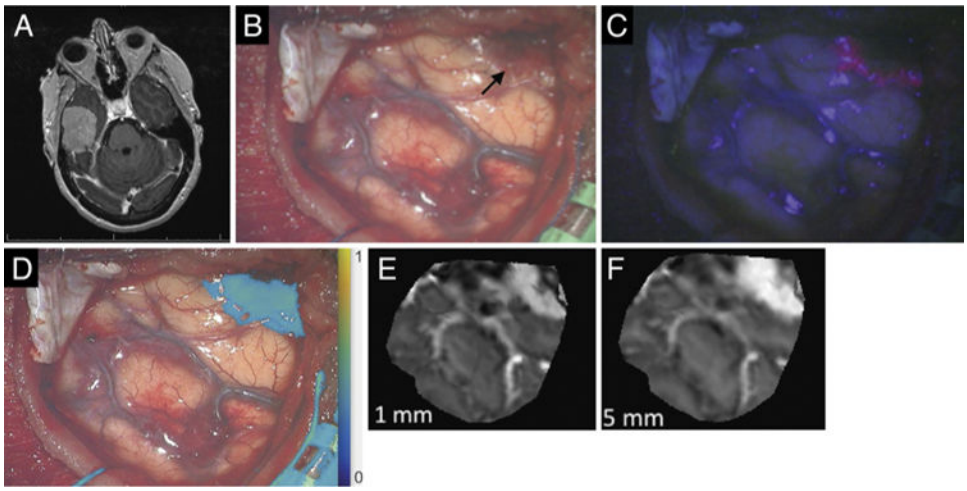

FIG. 5.

Case 11. **A:** Axial contrast-enhanced T1-weighted MR image of a well-demarcated tumor consistent with meningioma, arising from the floor of the right middle fossa. **B:** White-light image acquired upon initial exposure of the tumor (*black arrow*). **C:** Blue-light fluorescence image of the same surgical field. **D:** Overlay of fluorescence under red-light excitation. **E:** Reconstruction of MRI data corresponding to a weighted average of the first 1 mm below the surface of the surgical field. **F:** Reconstruction of weighted MRI data corresponding to the first 5 mm below the surface of the surgical field.

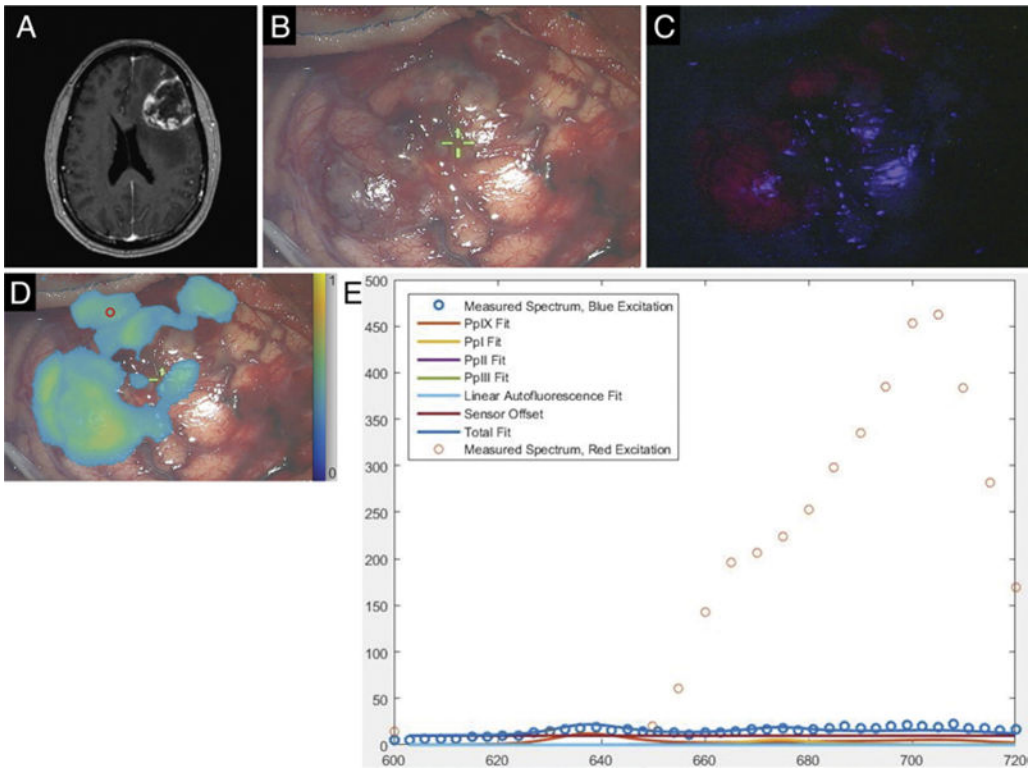

FIG. 6.

Case 24. **A:** Axial 3D MPRAGE image obtained after gadolinium administration, showing a heterogeneously contrast-enhancing, left frontal mass lesion. **B:** White-light image of tumor-involved cortical surface. **C:** Blue-light excitation fluorescence image of the same surgical field demonstrating fluorescence in areas of obvious tumor involvement. **D:** Map of PpIX fluorescence detected during red-light illumination superposed on a white-light image of the surgical field. The *small red circle* in the upper left portion of the image corresponds to the region of interest interrogated with the handheld optical probe. **E:** Optical spectra and model fits for PpIX, photoproducts, and autofluorescence at the site indicated by the *small red circle* in panel D. The typical blue light–elicited PpIX emission peak at 635 nm is absent (confirming the absence of conventional red fluorescence signal under blue-light excitation), while emission at longer wavelengths detected under red-light excitation confirms the presence of PpIX.

TABLE 1

Intraoperative fluorescence in high-grade gliomas

Case No.	Histopathology	Blue Light (visual)	Blue Light (quantitative)	Red Light (spectrally fit)
3	GBM	3	3	3
4	GBM	2	3	3
5	GBM	2	2	2
8	GBM	2	2	2
9	Recurrent GBM	2	3	3
10	AOA	1	1	0
14	AA	0	1	0
15	Recurrent GBM	2	2	2
18	GBM	1	1	1
22	GBM	2	2	1*
24	GBM	3	3	3
26	Recurrent GBM	2	2	1

AA = anaplastic astrocytoma; AOA = anaplastic oligoastrocytoma; blue light (visual) = maximal visually perceived fluorescence under blue-light excitation; blue light (quantitative) = maximal PpIX concentration estimate using blue-light excitation, multispectral camera, and correction for optical properties; red light (spectrally fit) = maximal PpIX concentration estimate using red-light excitation and hyperspectral camera.

Visual fluorescence was graded as none (0), low (1), moderate (2), or high (3).

*Red-light image not acquired at site of maximum quantitative blue-light fluorescence.

TABLE 2

Intraoperative fluorescence in low-grade gliomas

Case No.	Hisbottomathology	Blue Light (visual)	Blue Light (quantitative)	Red Light (spectrally fit)
12	Astrocytoma	0	1	1
16	Astrocytoma	0	1	0*
20	Astrocytoma	0	0	0
28	Ganglioglioma	0	0	0
29	Ganglioglioma	0	0	0

*Red-light image not acquired at site of maximum quantitative blue-light fluorescence.

TABLE 3

Intraoperative fluorescence in meningiomas

Case No.	Histopathology	Blue Light (visual)	Blue Light (quantitative)	Red Light (spectrally fit)
1	Anaplastic meningioma (WHO III)	2	3	3
2	Meningothelial meningioma (WHO I)	2	2	3
11	Atypical meningioma (WHO II)	2	2	3
21	Fibrous meningioma (WHO I)	3	3	0
23	Meningioma (WHO I)	3	1	3
25	Meningioma (WHO I)	3	3	3

TABLE 4

Intraoperative fluorescence in metastases

Case No.	Histopathology	Blue Light (visual)	Blue Light (quantitative)	Red Light (spectrally fit)
6	Adenocarcinoma	2	1	1
7	Adenocarcinoma	2	2	1
19	Adenocarcinoma	2	1	1
27	Adenocarcinoma	1	1	1